A99-33421

AIAA-99-3207

SHOCK INTERFERENCE IN HYPERSONIC RAREFIED-GAS FLOWS NEAR A CYLINDER

Vladimir V. Riabov*
University of New Hampshire
Manchester, New Hampshire 03101, USA
and
Andrei V. Botin†
Central Aero-Hydrodynamics Institute (TsAGI)
Zhukovsky-3, Moscow Region 140160, Russia

Abstract

The interference of an impinging plane oblique shock wave with the viscous shock layer on a cylinder modeling a hypersonic inlet edge has been studied experimentally and numerically for rarefied-gas flow regimes at the Reynolds numbers $15.5 \le Re_0 \le 124$ and Knudsen numbers $0.1 \ge Kn \ge 0.012$. The numerical calculations have been performed within the framework of the Direct Simulation Monte-Carlo technique and the Navier-Stokes equations for a perfect gas using the shock capturing method. The principal properties of the flow-parameters distribution have been studied for five different types of interference at low Reynolds numbers. The differences with respect to the previously investigated interference regimes for high Reynolds numbers were examined as well. The comparison analysis of numerical results and experimental data has been provided. It has been found that the local pressure and heat transfer coefficients on the surface of a cylinder may considerably (by a factor of 3.5) exceed the values on the edge stagnation line observed in the absence of interference. The type IV of the interference patterns in continuum media has not been found in the study.

Nomenclature

C_f = local skin-friction coefficient, τ_w/q_∞
C_p = pressure coefficient, $(p_w - p_\infty)/q_\infty$
H = total enthalpy
M = Mach number
Kn_R = Knudsen number
p = pressure, N/m^2
q = heat flux
q_∞ = dynamic pressure, $0.5\rho_\infty u_\infty^2$
R = radius of a cylinder, 0.01 m
Re_0 = Reynolds number, $\rho_\infty u_\infty R/\mu(T_0)$
St = Stanton number, $q_w/c_p\rho_\infty u_\infty(T_0 - T_w)$
T = temperature, K
t_w = temperature factor, T_w/T_0
x, y = Cartesian coordinates
β = angle of inclination of the shock
γ = specific heat ration, 1.4
η = second curvilinear coordinate
φ = meridian angle, deg
μ = viscosity coefficient
θ = apex angle of a wedge, deg
ρ = density, kg/m^3
τ = stress, N/m^2
ξ = first curvilinear coordinate

subscripts

R = cylinder radius as a length-scale parameter
w = wall condition
0 = stagnation parameter
∞ = free-stream parameter

Introduction

The optimum flow rate through the air intake of a hypersonic vehicle would be obtained under a condition that the oblique shock wave from its forward section impinges on the blunt edge of the air intake[1,2]. At hypersonic continuum flow regimes, six types of interference between an impinging oblique shock and a viscous shock layer near a cylindrical blunt edge had been studied by Edney[3], Wieting and Holden[4], Borovoi[5], Borovoi et al.[6], Purpura et al.[7], and Tannehill, J. C., Holst, T. L., and Rakich, J.[8] The studies indicate that pressure and heat flux on the surface of the body may

*Lecture, College of Engineering and Physical Sciences, 400 Commercial Street. Member AIAA.
†Research Scientist, Rarefied Gas Dynamics Branch, Aerothermodynamics Division.

considerably exceed the values on the edge stagnation line in the absence of interference. The rarefied-gas hypersonic flow regimes had been analyzed in experiments of Botin[9] and Pot et al.[10]

In the present study, the interference of an impinging shock with the viscous shock layer on a cylinder modeling a hypersonic inlet edge has been studied experimentally and numerically for rarefied-gas flow regimes at the Reynolds numbers $15.5 \le Re_0 \le 124$ and Knudsen numbers $0.1 \ge Kn_R \ge 0.012$. The numerical results have been obtained using the direct simulation Monte Carlo (DSMC) technique[11] and the shock capturing method[12] applied to the system of the Navier-Stokes equations. The DSMC computer code[13] was developed by G. Bird. Results are compared with experimental data obtained in the vacuum wind tunnel.

Flow Patterns

We consider the interference of steady flow around an infinite circular cylinder and an impinging oblique shock in hypersonic stream of rarefied air. The plane oblique shock is generated by a wedge with an apex angle θ, and the angle of inclination of the shock β. The flow patterns over the cylinder had been discussed in detail by Edney[3], Borovoi[5], and Purpura et al.[7]

Let us suppose that the oblique shock meets the bow shock ahead of a cylinder at different locations generating the interference of different types:

a) Type I interference is characterized by the formation of two shocks after the intersection of two oblique shocks coming from opposite directions in the flow region located underneath the lower sonic line.
b) Type II interaction reflects the Mach phenomenon[3,5-7] and produces two triple points separated by a normal shock after the intersection of the two oblique shock waves.
c) If the oblique shock crosses the strong bow shock, a slip line is produced separating subsonic area from a supersonic flow zone. In the Type III interference case, the slip line reattaches on the body surface. This case would be only possible in continuum at small inclination angles, $\beta \le 20$ deg.[3,7]
d) If the slip line could not reattach on the wall, a supersonic jet flown in the subsonic region follows it (Type IV).[3,5] The special case of the curved supersonic jet (Type IVa) was studied by Purpura et al.[7]
e) Both weak oblique shock waves of the same direction would interact above the upper sonic line generating a supersonic jet after the upper multiple point (Type V).[7]
f) Far from the leading critical point of the cylinder, a shock, a slip line and an expansion wave would be generated behind the triple point above the considered region (Type VI).[5-7]

In continuum flow regime, the theory of shock polars[7,10] can be effectively used to predict the localization of the different interference types around a cylinder. In the present study, the similar technique has been employed to estimate boundaries of interaction zones, as well as upstream boundary locations.

Experimental Techniques and Results

The experiments have been carried out in a vacuum wind tunnel at low-density airflow parameters: $M_\infty = 6.5$, $T_0 = 1000$ K, $p_0 = 4000$ N/m^2, $t_w = 0.31$, and $\gamma = 1.4$. The model is a plate with a cylindrical edge of radius $R =$ 0.01 m. The flow can be characterized by similarity parameters: the Reynolds number $Re_0 = 15.5$ and the Knudsen number $Kn_R = 0.1$.

The plane oblique shock wave was generated by a wedge with an apex angle $\theta = 20$ deg, and the angle of the shock inclination β about 27 deg. A string transverse mechanism allowed moving the wedge at any position along the vertical Y-axis to simulate interactions.

The electron-beam fluorescence technique[9] was used for flow visualization. Five different cases of interference was found in the experiments (see Figs. 1a - 1e corresponding to Types I, II, III, V, and VI). The flow patterns would be compared with the flow near a cylinder in the non-interference case (see Fig. 1f).

The local heat flux to the model surface elements was measured by using the mono-layer thermal sensitive coating technique.[6,9,20] The accuracy of the heat-flux data was studied in detail by Ardasheva et al.[20] The data errors are approximately estimated as 20 percent in regions far from the leading critical point and up to 40 percent at the leading edge.

The distributions of the local Stanton number ratios St/St_0 are shown in Fig. 2a - 2e for the five types of shock-waves interactions.

The DSMC Method

The DSMC method[11] has been used in this study as a numerical simulation technique for low-density hypersonic gas flows. A two-dimensional DSMC code[13] is used in this study. Molecular collisions in air are modeled using the variable hard sphere (VHS) molecular

model[11]. The gas-surface interactions are assumed to be fully diffusive with full moment and energy accommodation. The code validation was tested by Riabov[16] in comparing numerical results with experimental data.[16,17]

In calculations, the total number of cells near a cylinder and wedge is 8400 in six zones, the molecules are distributed non-evenly,[18] and a total number of 60,000 molecules corresponds to an average 7 molecules per cell. Acceptable results are obtained for an average of at least ten molecules per cell in the most critical region of the flow.[11,13,18] The error was pronounced when this number falls below five (i.e., flow in the behind the wedge or cylinder). In all cases the usual criterion[18] for the time step Δt_m has been realized, $2\times10^{-7} \le \Delta t_m \le 1\times10^{-6}$ s. Under these conditions, heat flux, aerodynamic coefficients, and gas-dynamic parameters have become insensitive to the time step.

The location of the external boundary with the upstream flow conditions varies from $2.5R$ to $3.5R$. Calculations were carried out on a personal computer. The computing time of each variant was estimated to be approximately 10 - 60 h.

The Navier-Stokes Equations

The system of Navier-Stokes equations, analogous to that presented in Refs. 12, 19 have been solved numerically. The meridian angle φ is varied over the interval $-90 \le \varphi \le +90$ deg. The steady-state equations in the arbitrary curvilinear coordinate system $\xi = \xi(x, y)$, $\eta = \eta(x, y)$, where x and y are Cartesian coordinates, have been written in the form of conservation laws.[12,19]

The equations have been nondimensionalized with respect to the parameters of velocity, density, temperature and viscosity in upstream flow. The cylinder radius R is used as a characteristic length scale parameter. The main similarity parameters are the Reynolds number Re_0, the Mach number M_∞, and the temperature factor t_w.

The outer boundary is divided into two parts: one part with uniform free-stream conditions at the constant Mach number M_∞, and the other with the conditions behind an inclined plane shock.[14] The velocity slip and temperature jump effects[15] are considered at the body surface.

The numerical method had been described in detail in Refs. 9, 12, and 19. A set of the FORTRAN standardized programs[12] has been used to solve the problem. The grid contains 44 nodes related to the surface curvilinear coordinate ξ and 41 nodes along the normal η. The finite-difference scheme with the program modules has the second-order accuracy.

Numerical Results and Discussion

The numerical results received by the DSMC and Navier-Stokes techniques are presented in Fig. 2a - 2e in the form of a distribution of the local Stanton number ratio, St/St_0 on the cylindrical surface along the meridian angle φ. The types I, II, III, V, and VI out of the six known types of interference described in Refs. 3-7 have been found at the free-stream conditions of rarefied air ($Re_0 = 15.5$; $Kn = 0.1$; $M_\infty = 6.5$; $T_0 = 1000$ K; $t_w = 0.31$; $\theta = 20$ deg; and $\beta = 27$ deg).

Mach number contours obtained by the DSMC technique under the same airflow conditions are shown in Figs. 3a - 3c for Types II, III, and V of interactions. The similar contours obtained by the solution of the Navier-Stokes equations are shown in Figs. 4a and 4b.

Type I interference is shown in Fig. 2a. The stagnation point has almost returned to its position in the absence of interference. No inhomogeneities of the shock wave or mixing layer type has been found in the shock layer. The heat transfer coefficient distribution also tends to the distribution obtained in the absence of interference.

Type II interference is shown in Fig. 2b. This type of interaction is observed when the oblique shock impinges on the supersonic region of the shock layer below the regular stagnation point. In this regime at high Reynolds numbers, a subsonic jet, bounded by the surfaces of the mixing layers departing from the lower and upper triple points, is formed within the supersonic flow in the shock layer[8]. An inner shock also departs from the upper triple point, crossing the shock layer to the surface of the cylinder. At high Reynolds numbers in the zone of impingement of this shock (i.e., in the mixing layer attachment zone) on the boundary layer there is a sharp increase in the pressure and heat flux to the surface of the blunt body.

At moderate Reynolds numbers, vizualization[5] and analysis of numerical data do not reveal inner shocks and mixing layers in the viscous shock layer. Only the change of shock layer configuration related to the type II interference has been observed. The stagnation point is displaced significantly downwards along the surface coordinate. In the vicinity of the stagnation point, both in the calculations and in the experiments[5], the local heat flux have maximum value. However, their absolute values are smaller than the corresponding values of heat flux under conditions of types III, V, and VI.

The type III interference is shown in Figs. 2c. According to Refs. 3, 6, and 8, the type III interference occurs when the inclined shock intersects the part of the

bow shock normal to the free-stream velocity vector. The calculated Mach number contours for the type III interference are presented in Figs. 3b and 4a. Experimental data[5-6] and analysis of the contours indicate that a secondary thick shock relocates from the lower triple point towards the surface of the body. However, the mixing layers are weakly expressed at the rarefied-gas flow regimes.

According to the study of Tannehill, Holst, and Rakich[8], at high Reynolds numbers the pressure and heat flux maximum values correspond to the region of impingement of the secondary shock on the boundary layer (the type III of interference). At moderate Reynolds numbers, it has been found that the maximum values of the heat flux are attained not in the surface-secondary-shock interaction zone but, as before, in the vicinity of the stagnation point displaced in the direction of negative φ. In this flow regime, the greatest increase in the maximum value of the heat flux is observed as compared with regular flow without interference (see Fig. 2c).

In our study, the type IV interference described in Refs. 3-8, which occurs at high Reynolds numbers and is characterized by the greatest values of the maximum pressure and heat flux, is not found at low Reynolds numbers. At low Reynolds numbers, when the shock layer is completely viscous and boundaries of mixing layers and the inner shocks in the viscous shock layer are thick, it appears that no supersonic jet is formed. Therefore as the wedge is displaced downwards along the Y-axis the type V interference goes over into type III, bypassing type IV.

The substantial differences between the flow patterns of the type V interference at high Reynolds numbers (Refs. 5, 8) and at low Reynolds numbers are found in this study. The cause of the local increase in the pressure and the heat flux to the body surface at high Reynolds numbers is the interaction between the secondary shock passing through the bow shock wave and the boundary layer on the body. At low Reynolds numbers the entire region from the bow shock to the body is a thick viscous shock layer. In this case, the secondary shock dissipates in the shock layer and no longer causes a local increase in the pressure and the heat flux to the surface. No secondary shock had been observed in experiments.

The numerical solutions of the Navier-Stokes equations allow the analysis of the flow structure in detail. The calculated Mach number contours for the type V interference are presented in Figs. 3c and 4b. Significant changes of the flow structure can be observed in the area below the shock intersection point. The level of air compression in this zone is much higher than behind the bow shock wave in the absence of interference. It results in increasing the heat flux by approximately 20% in the vicinity of the leading stagnation point (see Fig. 2d).

Figure 2e shows the type VI interference that results when the oblique shock impinges on the upper supersonic region of the shock layer at a sufficient distance from the stagnation point above it. Behind the interference zone the shock layer thickness increases significantly, since the flow behind the oblique shock affects almost the entire region in front of the blunt body. This leads to a redistribution of the flow parameters in the shock layer and to a change in its structure. The stagnation point is displaced into the region of negative φ. In the vicinity of this point there is a significant increase in the values of the local heat flux. The calculated results are compared with experimental data[9] (circles) and the distributions of the calculated values of the local Stanton numbers in the absence of interference (dashed line). At $\varphi < -35$ deg the experimental values of the local heat flux are significantly lower than the calculated values. In experiments provided by the thermal indicator coating method[20], the study region lies in the zone of the wake expanded from the trailing edge of the wedge. This feature is also present, although to a smaller error, in Fig. 2d, which corresponds to the type V interference.

Distributions of the pressure and local skin-friction coefficients for this flow regime and different types of interference are shown in Figs. 7 and 8.

Cases of the Moderate Reynolds Numbers

Numerical data obtained by the DSMC technique have been studied at the free-stream conditions of rarefied air ($Re_0 = 124$; $Kn = 0.012$; $M_\infty = 6.5$; $T_0 = 1000$ K; $t_w = 0.31$; $\theta = 20$ deg). Mach number contours and streamlines are shown in Figs. 3a - 3c for the Type III of interaction. Thickness of the oblique and bow shocks becomes smaller in comparison with the shock thickness in rarefied-gas flow regime. The effective angle of the oblique shock becomes smaller as well, because of the reduction of the boundary layer at the wedge surface.

This cause results in moving the actual stagnation point down (see Figs. 9a, 10a, 11a). For other interference types this phenomenon is not pronounced (see Figs. 9b, 10b, 11b for the Type II).

Conclusion Remarks

The different types of interference between the impinging plane oblique shock wave and the shock layer near a cylinder have been studied at low and moderate

Reynolds numbers. It has been found that the type IV interference does not take place in the flow regimes studied in experiments and by the direct simulation Monte-Carlo technique and the numerical solutions of the Navier-Stokes equations. Interference of this type occurs only at high Reynolds numbers when the inclined shock impinges on the part of the bow shock almost perpendicular to the free-stream velocity vector. In this case the gas passing through the system of oblique secondary shocks forms a supersonic jet, in which the total pressure is much higher than in the surrounding subsonic flow. For types VI, V, and III of interference, the local pressure and heat flux parameters on the cylinder surface considerably exceed the values in the absence of interference. This fact is in a good agreement with known experimental and analytical results.

References

[1]Billig, F. S., "Research on Supersonic Combustion," *Journal of Propulsion and Power*, Vol. 9, No. 4, July-Aug. 1993, pp. 499-514.

[2]Gusev, V. N., "High-Altitude Aerothermodynamics," *Fluid Dynamics*, Vol. 28, No. 2, 1993, pp. 269-276.

[3]Edney, B., "Anomalous Heat Transfer and Pressure Distributions on Blunt Bodies at Hypersonic Speeds in the Presence of an Impinging Shock", Aeronautical Research Institute of Sweden, FFA Report 115, Stockholm, 1968.

[4]Wieting, A. R., and Holden, M. S., "Experimental Shock-Wave Interference Heating on a Cylinder at Mach 6 and 8," *AIAA Journal*, Vol. 27, No. 11, 1989, pp. 1557-1565.

[5]Borovoi, V. Ya, *Gas Flow and Heat Transfer in Shock Wave-Boundary Layer Interaction Zones*, 1st ed., Mashinostroenie, Moscow, 1983, p. 141 (*in Russian*).

[6]Borovoi, V. Ya, Chinilov, A. Yu., Gusev, V. N., Struminskaya, I. V., Délery, J., and Chanetz, B., "Interference Between a Cylindrical bow Shock and a Plane Oblique Shock," *AIAA Paper*, No. 96- 2374, June 1996.

[7]Purpura, C., Chanetz, B., Délery, J., and Grasso, F., "Type III and Type IV Shock/Shock Interference's: Theoretical and Experimental Aspects," *Proceeding of the 21st International Symposium on Rarefied Gas Dynamics*, Marseille, France, 1998, pp. 1-8.

[8]Tannehill, J. C., Holst, T. L., and Rakich, J., "Numerical Calculations of a Two-Dimensional Viscous Blunt Body Flows with an Impinging Shock," *AIAA Journal*, Vol. 14, No. 2, 1976, pp. 204-211.

[9]Botin, A. V., "Interference between a Blunt Edge Shock Layer and an Impinging Inclined Shock at Low Reynolds Numbers," *Fluid Dynamics*, Vol. 28, No. 1, 1993, pp. 126-130.

[10]Pot, T., Chanetz, B., Lefebvre, M., and Bouchardy, P., "Fundamental Study of Shock/Shock Interference in Low Density Flow: Flowfield Measurements by DLCARS," *Proceeding of the 21st International Symposium on Rarefied Gas Dymanics*, Marseille, France, 1998, pp. 1-8.

[11]Bird, G. A., *Molecular Gas Dynamics and the Direct Simulation of Gas Flows*, 1st ed., Oxford University Press, Oxford, 1994, pp. 340-377.

[12]Egorov, I. V., and Zaitsev, O. L., "On an Approach to the Numerical Solution of the Two-Dimensional Navier-Stokes Equations by the Shock-Capturing Method," *Journal of Computational Mathematics and Mathematical Physics*, Vol. 31, No. 2, 1991, pp. 286-299.

[13]Bird, G. A., "The DS2G Program User's Guide, Version 1.0," G.A.B. Consulting Pty, Killara, New South Wales, Australia, 1995.

[14]Anderson, J. D., Jr., *Hypersonic and High Temperature Gas Dynamics*, 1st ed., McGraw-Hill, New York, 1989.

[15]Kogan, M. N., *Rarefied Gas Dynamics*, 1st ed., Plenum Press, New York, 1969.

[16]Riabov, V. V., "Comparative Similarity Analysis of Hypersonic Rarefied Gas Flows near Simple-Shape Bodies," *Journal of Spacecraft and Rockets*, Vol. 35, No. 4, 1998, pp. 424-433.

[17]Gusev, V. N., Erofeev, A. I., Klimova, T. V., Perepukhov, V. A., Riabov, V. V., and Tolstykh, A. I., "Theoretical and Experimental Investigations of Flow Over Simple Shape Bodies by a Hypersonic Stream of Rarefied Gas," *Trudy TsAGI*, Issue 1855, 1977, pp. 3-43 (in Russian).

[18]Bird, G. A., "A Rarefied Hypersonic Flow Past a Slender Sharp Cone," *Proceedings of the 13th International Symposium on Rarefied Gas Dynamics*, Vol. 1, Plenum Press, New York, 1985, pp. 349-356.

[19]Yegorov, I. V., Yegorova, M. V. Ivanov, D. V., and Riabov, V. V., "Numerical Study of Hypersonic Viscous Flow About plates Located Behind a Cylinder", *AIAA Paper*, No. 97-2573, June 1997.

[20]Ardasheva, M. M., Klimova, T. V., Pervushin, G. V., and Chernikova, L. G., "Study of Local Heat Fluxes by Means of the Thermal Indicator Coating Method," *Trudy TsAGI*, Issue 2111, 1981, pp. 197-207 (*in Russian*).

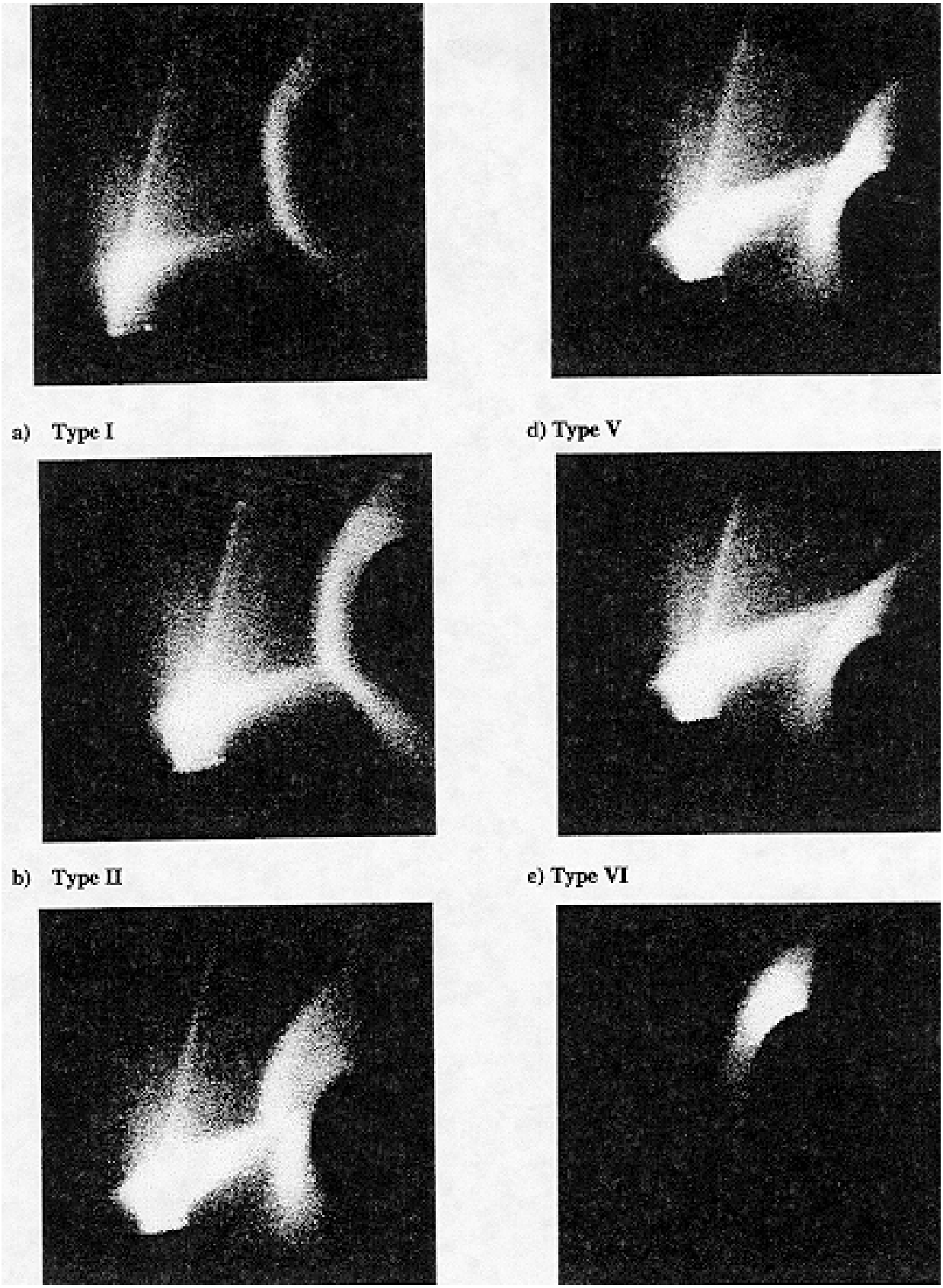

Fig. 1 Visualization of different type interactions by electron-beam fluorescence at $Re_0 = 15.5$ ($Kn_R = 0.1$): a) type I, b) type II, c) type III; d) type V, e) type VI, and f) no interference.

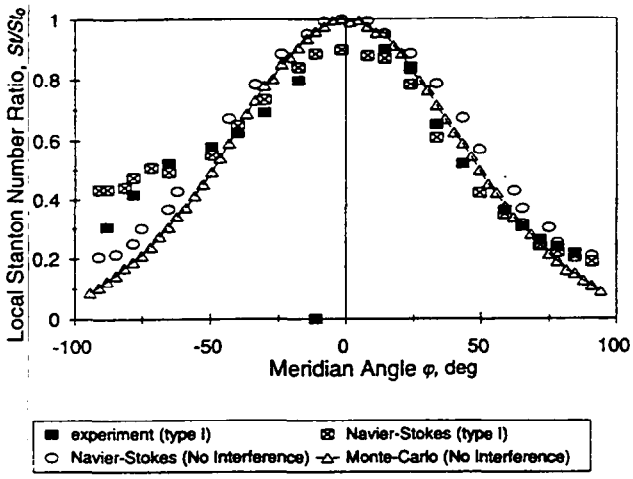

a) Type I

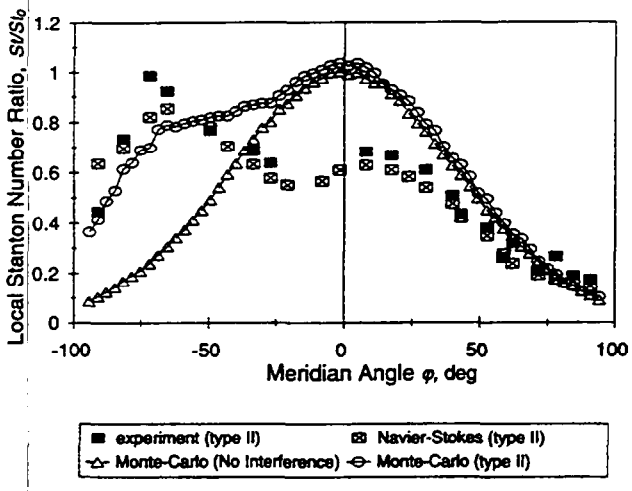

b) Type II

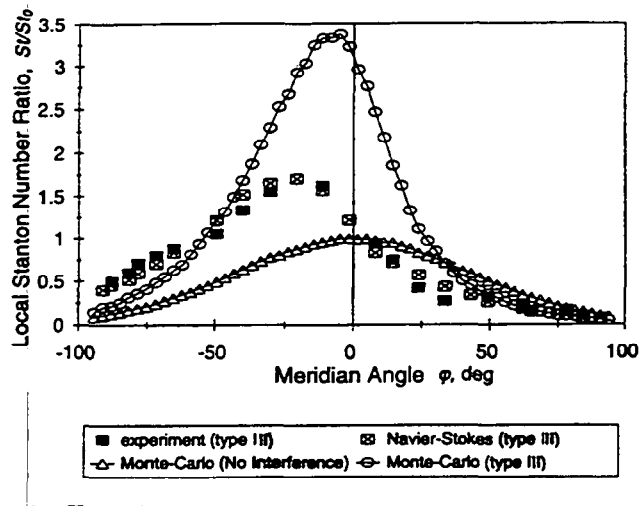

c) Type III

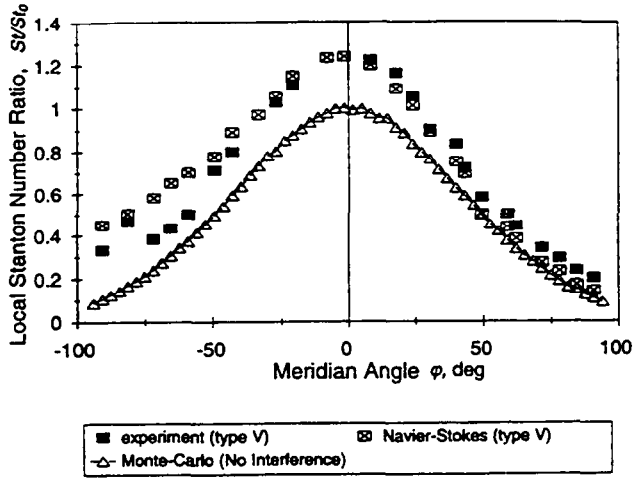

d) Type V

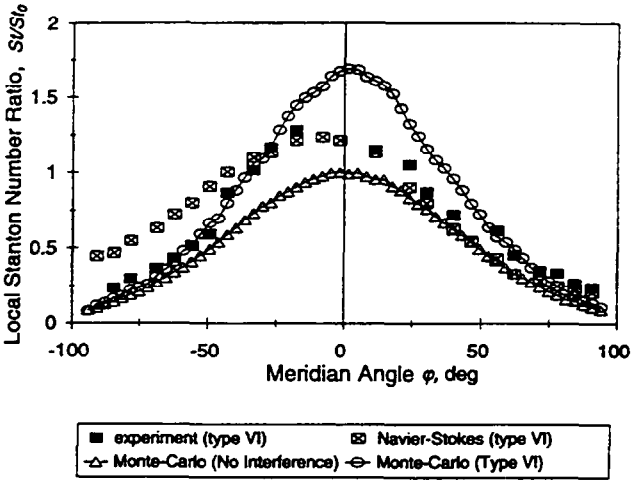

e) Type VI

Fig. 2 Comparison between experimental and numerical results of local Stanton number ratio distributions around a cylinder at $Re_0 = 15.5$ ($Kn_R = 0.1$) for different types of shock/shock layer interference: a) type I; b) type II; c) type III; d) type V, and e) type VI.

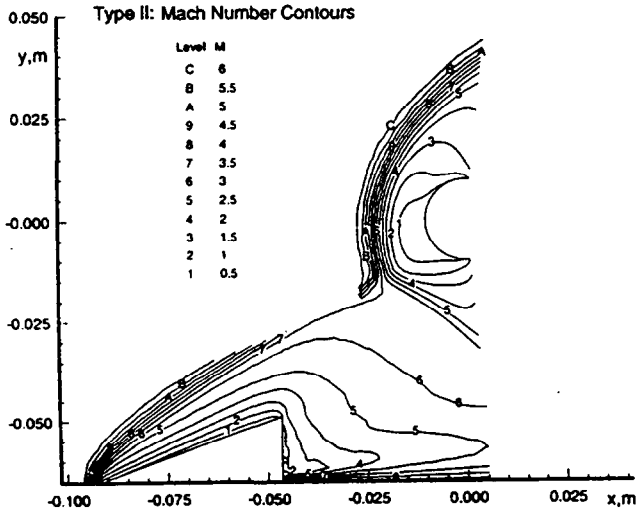

a) Type II

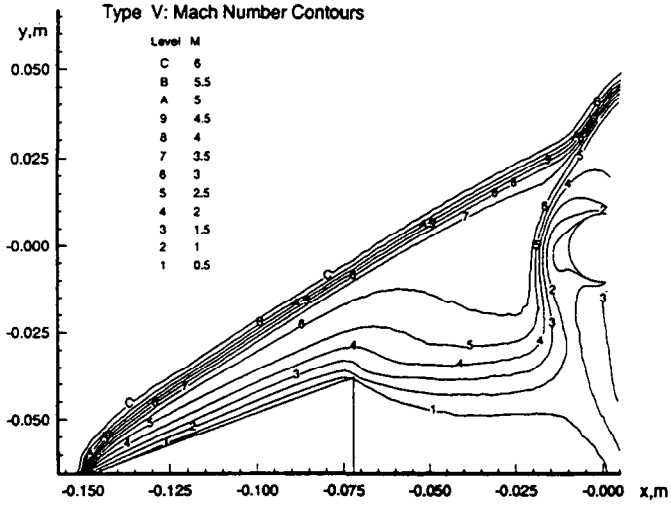

c) Type V

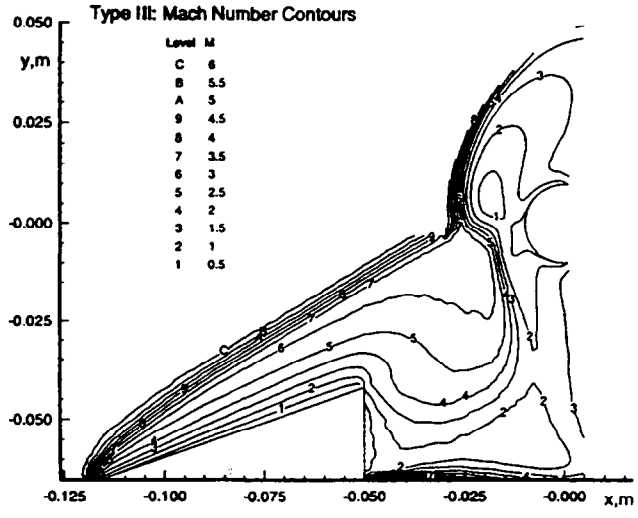

b) Type III

Fig. 3 Mach number contours calculated by the DSMC technique at $Re_0 = 15.5$ ($Kn_R = 0.1$) for different types of interaction: a) type II, b) type III, and c) type V.

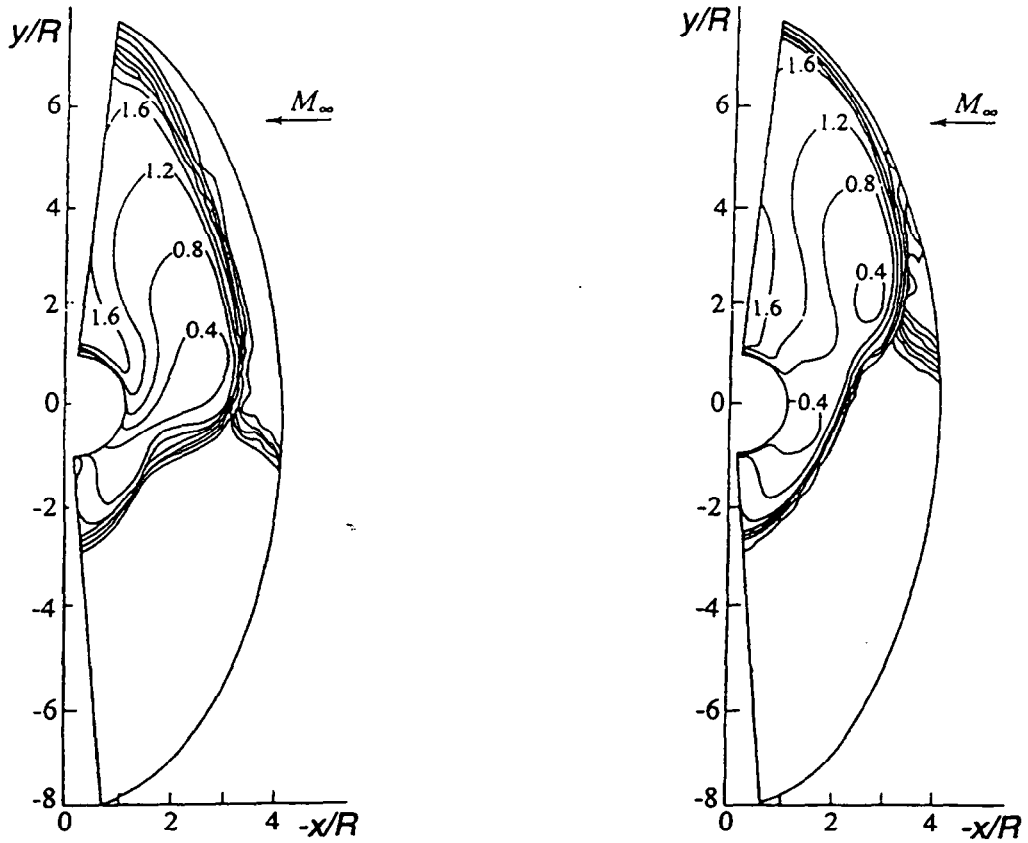

a) Type III

b) Type V

Fig. 4 Mach number contours calculated by the Navier-Stokes technique at $Re_0 = 15.5$ ($Kn_R = 0.1$) for different types of interaction: a) type III; b) type V.

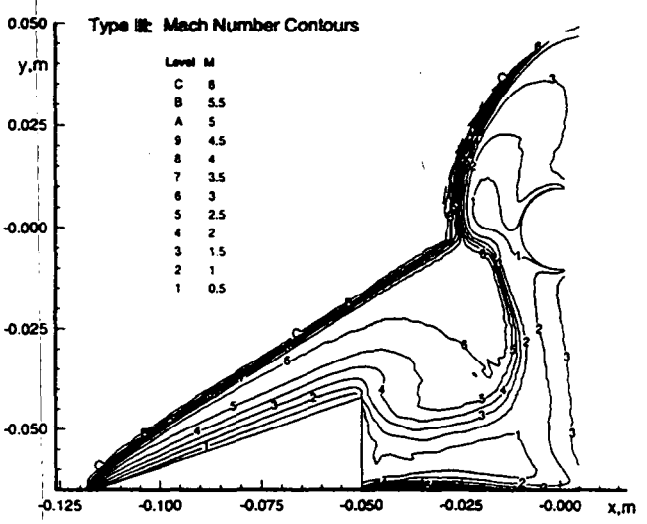

Fig. 5 Mach number contours calculated by the DSMC technique at $Re_0 = 124$ ($Kn_R = 0.012$) for the type III interaction.

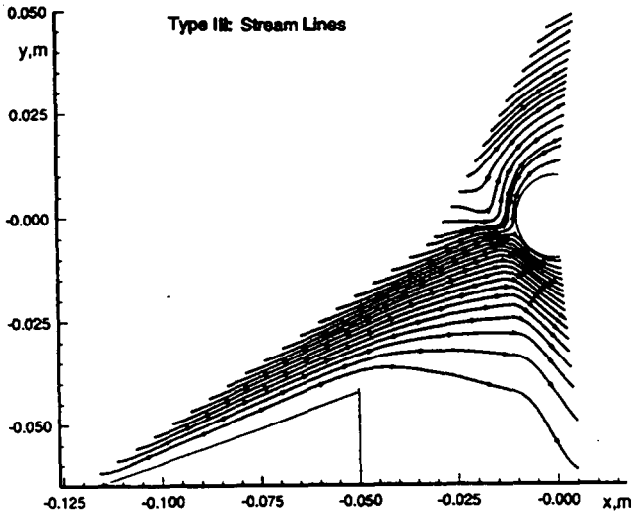

Fig. 6 Streamlines calculated by the DSMC technique at $Re_0 = 124$ ($Kn_R = 0.012$) for the type III interaction.

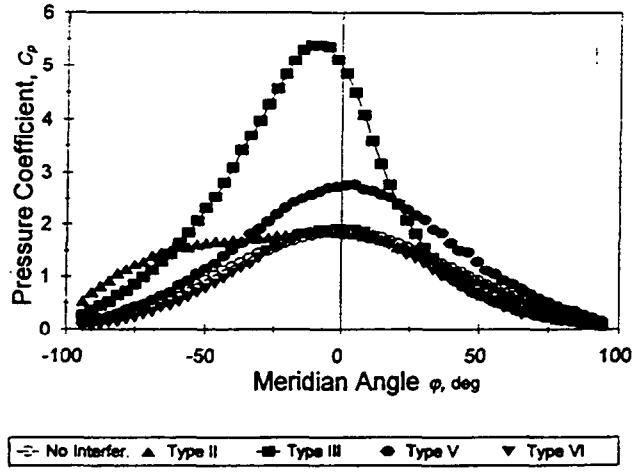

Fig. 7 Local pressure coefficient distributions around a cylinder at $Re_0 = 15.5$ ($Kn_R = 0.1$) for different types of shock/shock layer interference.

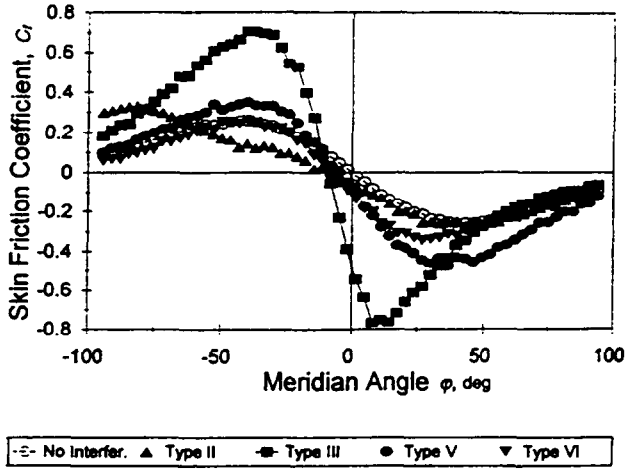

Fig. 8 Local skin friction coefficient distributions around a cylinder at $Re_0 = 15.5$ ($Kn_R = 0.1$) for different types of shock/shock layer interference.

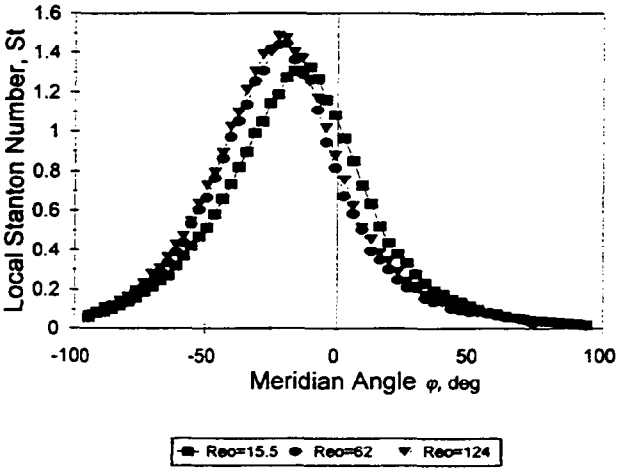

a) Type III

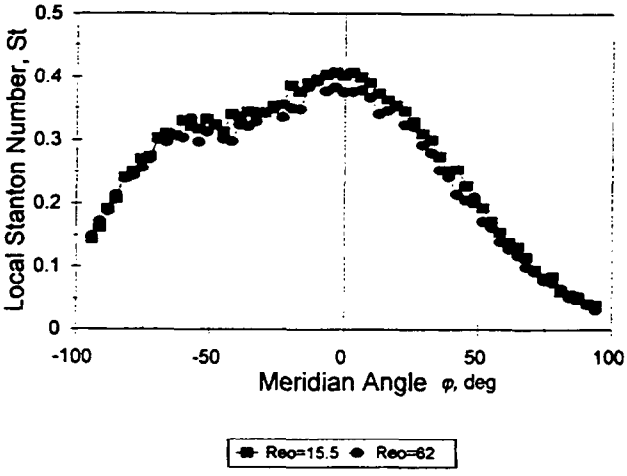

b) Type II

Fig. 9 Local Stanton number distributions around a cylinder at various Reynolds numbers for different types of shock/shock layer interference: a) type III; b) type II.

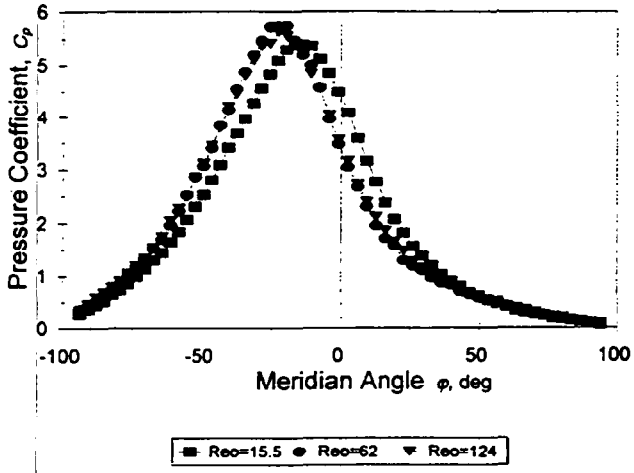

a) Type III

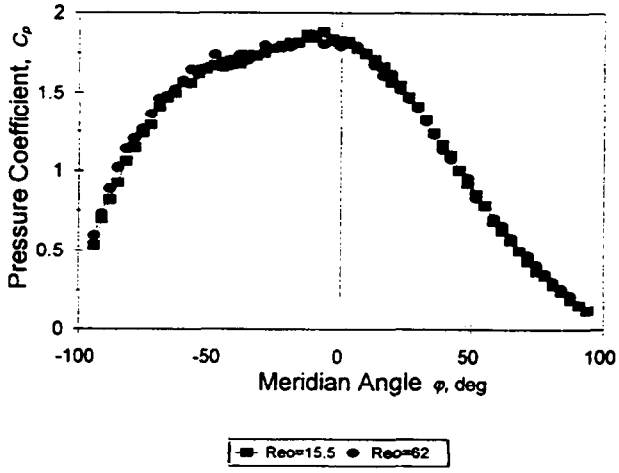

b) Type II

Fig. 10 Local pressure coefficient distributions around a cylinder at various Reynolds numbers for different types of shock/shock layer interference: a) type III; b) type II.

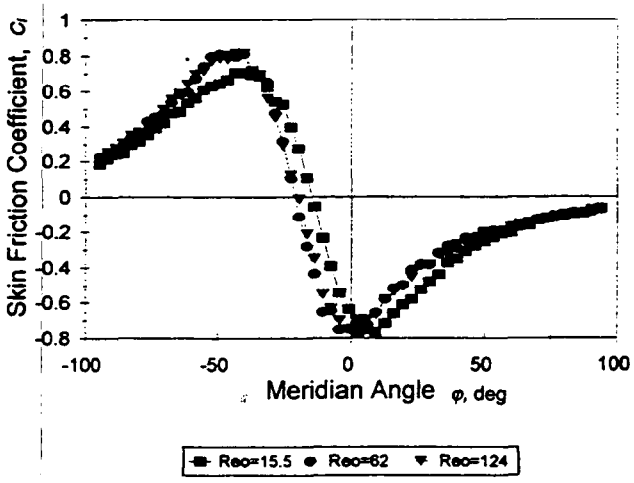

a) Type III

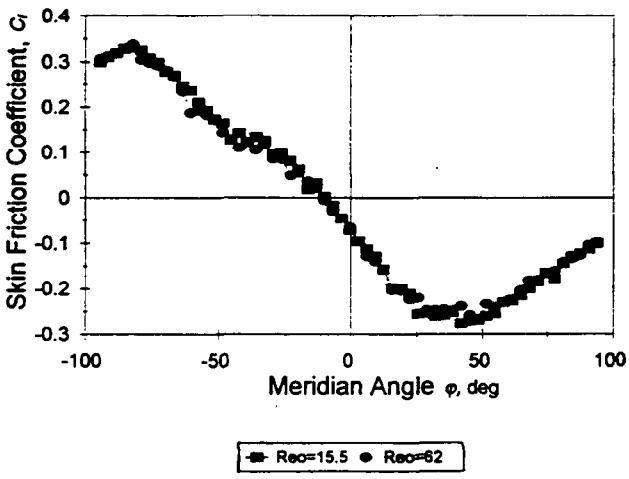

b) Type II

Fig. 11 Local skin friction coefficient distributions around a cylinder at various Reynolds numbers for different types of shock/shock layer interference: a) type III; b) type II.